# Inside the whale: the structure and dynamics of the isolated Cetus dwarf spheroidal

G. F. Lewis,[1]⋆ R. A. Ibata,[2] S. C. Chapman,[3] A. McConnachie,[4] M. J. Irwin,[5] E. Tolstoy[6] and N. R. Tanvir[7]

[1]*Institute of Astronomy, School of Physics, A28, University of Sydney, NSW 2006, Australia*
[2]*Observatoire de Strasbourg, 11, rue de l'Universit, Strasbourg F-67000, France*
[3]*California Institute of Technology, Pasadena, CA 91125, USA*
[4]*Department of Physics & Astronomy, University of Victoria, Victoria, BC VP8 1A1, Canada*
[5]*Institute of Astronomy, Madingley Road, Cambridge CB3 0HA*
[6]*Kapteyn Institute, University of Groningen, Postbus 800, 9700 AV Groningen, the Netherlands*
[7]*Physical Science, University of Hertfordshire, Hatfield AL10 9AB*

**ABSTRACT**
This paper presents a study of the Cetus dwarf, an isolated dwarf galaxy within the Local Group. A matched-filter analysis of the INT/WFC imaging of this system reveals no evidence for significant tidal debris that could have been torn off the galaxy, bolstering the hypothesis that Cetus has never significantly interacted with either the Milky Way or M31. Additionally, Keck/Deimos spectroscopic observations identify this galaxy as a distinct kinematic population possessing a systematic velocity of $-87 \pm 2\,\mathrm{km\,s^{-1}}$ and with a velocity dispersion of $17 \pm 2\,\mathrm{km\,s^{-1}}$; while tentative, these data also suggest that Cetus possesses a moderate rotational velocity of $\sim 8\,\mathrm{km\,s^{-1}}$. The population is confirmed to be relatively metal-poor, consistent with [Fe/H] $\sim -1.9$, and, assuming virial equilibrium, implies that the Cetus dwarf galaxy possesses a mass-to-light ratio of $\sim 70$. It appears, therefore, that Cetus may represent a primordial dwarf galaxy, retaining the kinematic and structural properties lost by other members of the dwarf population of the Local Group in their interactions with the large galaxies. An analysis of Cetus' orbit through the Local Group indicates that it is at apocentre; taken in conjunction with the general dwarf population, this shows the mass of the Local Group to be $\gtrsim 2 \times 10^{12}\,\mathrm{M_\odot}$.

**Key words:** galaxies: dwarf – galaxies: individual: Cetus – Local Group.

## 1 INTRODUCTION

Within the cold dark matter paradigm, galaxies grow over time through the continued accretion of smaller systems (White & Rees 1978). Dwarf galaxies, therefore, being at the bottom of this hierarchical formation picture (or food chain), are amongst the most 'fundamental' of galactic building blocks. While recent metallicity observations of Local Group dwarf galaxies have suggested that the Milky Way could not have formed from systems resembling the current dwarf population (Venn et al. 2004), current accretion events in the Milky Way (Ibata, Gilmore & Irwin 1994; Martin et al. 2004) and Andromeda Galaxy (Ibata et al. 2001) illustrate that the galaxy formation process is still ongoing, albeit at a gentle pace.

Dwarf galaxies remain the dominant population of galaxies in the Universe; while the Local Group contains only two dominant, large galaxies (Milky Way and M31), the population of dwarf galaxies

numbers more than 40 (Mateo 1998). The advent of deep, panoramic surveys of the Local Group has recently revealed several more examples of these galaxies (Zucker et al. 2004; Willman et al. 2005a,b; Belokurov et al. 2006a,b; Zucker et al. 2006a,b), but still the apparent conflict between the expected and observed population of dwarf galaxies remains (Klypin et al. 1999; Moore et al. 1999). The theoretical and observational picture can be brought into agreement if star formation in low-mass systems is suppressed via such mechanisms as photoionization in the early universe, leaving only a meager stellar population to reveal their location. Such models, however, predict that dwarf galaxies should be enveloped in massive haloes of dark matter (Stoehr et al. 2002); such haloes would be revealed in the stellar kinematics of the dwarf at large radii.

Dwarf spheroidal galaxies (generally gas-poor, pressure-supported systems) are preferentially found as satellites to the Milky Way and M31, whereas dwarf irregular galaxies (generally gas rich, rotating systems) are preferentially found as isolated systems. This position–morphology relation was first highlighted by Einasto, Kaasik & Saar (1974) and suggests that the environment of a dwarf

⋆E-mail: gfl@physics.usyd.edu.au

galaxy plays a fundamental role in driving its evolution. Mayer et al. (2001a,b, 2006) suggested that tidal effects and ram pressure stripping of dwarf galaxies in the halo of large galaxies may be sufficient to turn a rotationally supported system into a pressure-supported system. Isolated dwarf spheroidals are, therefore, particularly interesting as they would have been immune for the shaking and stirring that has occurred to most dwarf systems and hence may represent the dwarf galaxies in their most pristine form. However, such isolated dwarf spheroidal galaxies are rare within the Local Group, with two dwarfs not currently a satellite of either the Milky Way and M31; Cetus and Tucana.[1] Determining the dynamical properties and orbital history of such galaxies can help determine the role of interactions in governing a dwarf galaxy's morphology.

Discovered by Whiting, Hau & Irwin (1999) in an eye-ball survey of photographic plates, the Cetus dwarf galaxy is seen to lie at a distance of $755 \pm 23$ kpc [McConnachie et al. 2005, assuming $E(B - V) = 0.029$]; it is almost as remote from M31, with a separation of 680 kpc. Hence, unlike the vast majority of dwarf systems within the Local Group, Cetus does not appear to be part of the entourage of either the Milky Way or Andromeda Galaxy, and apparently represents an isolated member of the local dwarf population. Furthermore, an analysis of the stellar distribution in this dwarf reveals it to possess a half-light radius of more than 300 pc, and a tidal radius of 6.6 kpc,[2] making it the largest radial extent dwarf within the local population (McConnachie & Irwin 2006). Such a large physical extent suggests that Cetus has not undergone a significant interaction with other members of the Local Group and hence provides an ideal testbed for kinematic analysis. To this end, a reanalysis of the INT/WFC data obtained by McConnachie et al. (2005) was undertaken to search for any evidence of tidal disruption due to any previous interactions. This was coupled with a spectroscopic survey of the Cetus dwarf galaxy which was undertaken with Deimos on the Keck 10-m telescope with the goal of determining its kinematic and dark matter properties. The details of the observations are presented in Section 2, while a discussion of the results appears in Section 3. This paper closes with Section 4 which presents the implications and conclusions of this study.

## 2 OBSERVATIONS

### 2.1 Photometric

The photometric observations were obtained with the INT/WFC on the 2.5-m Isaac Newton Telescope on La Palma and were originally presented by McConnachie et al. (2005). As noted in this previous work, the *V* and *I* colour–magnitude diagram (CMD) of the Cetus dwarf clearly reveals the presence of a red giant branch (RGB) below $I = 20.5$. Furthermore, the presence of the dwarf is clearly revealed in stellar density, as apparent in Fig. 1. Hence, these photometric data were used to select targets for spectroscopic follow-up with the Keck telescope. The stars were chosen to lie within ~0.15 mag of the RGB between $22.0 < I < 20.5$; the selection box is overlain on the CMD presented in Fig. 2 and the spatial distribution of stars
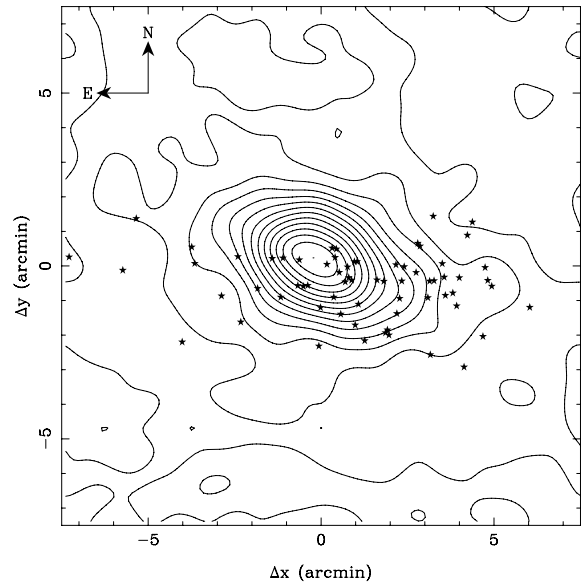
---

[1] The transition-type dwarf spheroidal/irregular, DDO210, lies ~1 Mpc from both M31 and the Milky Way, and may be interacting with the Local Group for the first time (McConnachie et al. 2006).

[2] As noted in McConnachie & Irwin (2006), the tidal radius for Cetus is very poorly constrained, with no significant turnover in the surface brightness profile at the largest radii probed. If it has had no interaction, the tidal radius may not represent a physical limit to Cetus.



**Figure 1.** The contours in this figure denote the stellar density in the Cetus dwarf galaxy as derived from INT/WFC imaging, centred on $\alpha = 00^h26^m11^s \, \delta = -11°02'40''$ (J2000) (see McConnachie & Irwin 2006). The star symbols represent the locations of the stars which form the basis of this study.

appears in Fig. 1. The selection box was extended to $I = 20$ to include candidate asymptotic giant branch stars into the sample.

### 2.2 Spectroscopic

Observations were undertaken with the DEIMOS spectrograph (Faber et al. 2003) on the 10-m W. M. Keck-II telescope in Hawaii on the night of 2005 October 1. The $1200 \, l \, mm^{-1}$ grating was blazed to 800 nm and, coupled with the OG550 order-blocking filter, provided an effective spectral range from 700 to 900 nm, encompassing the calcium II triplet (CaT); it is this series of lines that provide kinematic and overall abundance ([Fe/H]) measures.

Custom-made slit masks were used to target stars in the Cetus dwarf galaxy; as noted previously, the astrometry was drawn from the INT/WFC survey presented in McConnachie et al. (2005), and the target field is shown overlain on the stellar density map of the dwarf in Fig. 1. The fields were flat-fielded and sky-subtracted as part of the standard Deimos data-reduction pipeline, while spectra were extracted using a dedicated software package (e.g. Ibata et al. 2005). Finally, velocities were calculated via cross-correlation of the spectra with zero-velocity stellar templates, utilizing the CaT, centred at ~8550 Å. This resulted in 70 stars with a velocity error less than $20 \, km \, s^{-1}$ with a mean (median) velocity error of 8.8 (7.7) $km \, s^{-1}$; the data from these stars are presented in Tables 1(a) and (b).

While the standard velocity errors are well understood, it is important to estimate any potential systematic uncertainties that may result from the reduction procedure. To this end, fake stellar spectra in the region of the CaT were generated, using sky residuals determined from Poisson sampling of the median observed sky spectrum. The resultant synthetic spectra possessed a signal-to-noise ratio (S/N) of ~5 and were analysed in the same fashion as the real data. The extracted velocity is compared to the input velocity in Fig. 3; in this figure, the top panel presents the results from synthetic spectra generated using the overall median sky spectrum, whereas the lower panel utilized median sky spectra from separate CCDs and hence
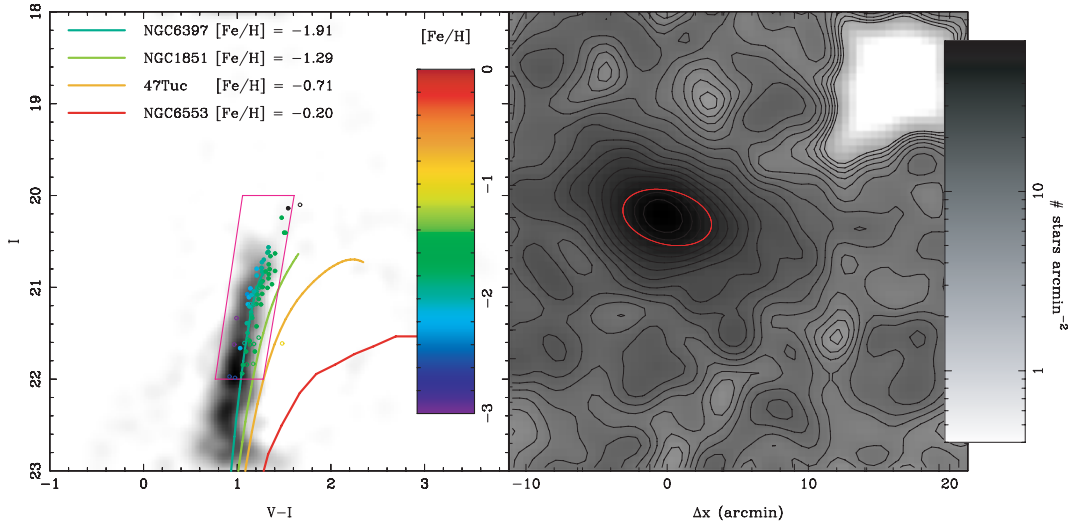
**Figure 2.** The left-hand panel presents the match filter weight map, constructed by dividing the CMD within the central 3 arcmin of the Cetus dwarf by the CMD from the region beyond 10 arcmin of the dwarf; this enhances the CMD signature of the dwarf. The isochrones from several fiducial systems are overplotted for comparison. The closed box denotes the selection region as described in Section 2.1, while the grey-scale circles (colour online) represent the observed stars, with the solid circles representing those within 30 km s$^{-1}$ of the systemic velocity of Cetus. The grey-scale coding represents the spectroscopically determined metallicity, as described in Section 3.3 and defined by the key. The right-hand panel presents the logarithm of the stellar density as identified by the matched filtering analysis. The peak value is ∼70 stars arcmin$^{-2}$, with each contour corresponding to 0.11 dex; this is also represented in the grey-scale as given in the key. The ellipse (red online) corresponds to the stellar peak seen in Fig. 1, whereas the square region in the upper right-hand corner represents the region not covered by the INT/WFC field.

represents a more extreme estimate of the sky residuals. It can be seen that in the region from $-100 \rightarrow 0$ km s$^{-1}$, the upper panel reveals small systematic uncertainties (∼1 km s$^{-1}$), whereas the lower panel displays more significant uncertainties of ∼4–5 km s$^{-1}$. It can be concluded that in this region the systematic uncertainties in the velocity determination are roughly half the value of the mean standard error.

## 3 RESULTS

### 3.1 Photometric search for extratidal stars

Given its remote location, Cetus appears to have lived a rather isolated existence, free from the large galactic tides that have influenced other dwarf galaxies. However, given the uncertainty of its orbit, its detailed historical motion through the Local Group is unknown and there is the possibility that it underwent interactions with other members in the past. The result of such interactions would depend on the specifics of the collisions, although it would be expected that if it interacted with a substantial system then the tidal disruption would result in the formation of tidal tails which could still accompany the dwarf today (e.g. Johnston, Choi & Guhathakurta 2002).

Tidal debris, however, typically presents a very low surface brightness and is not apparent in maps of stellar density. However, various statistical techniques exist that allow the extraction of low surface brightness features by identifying the sequence of the dwarf within an overall background CMD. To this end, a matched filter analysis (Kepner et al. 1999; Rockosi et al. 2002) of the INT/WFC data of the Cetus dwarf was undertaken; for this, a background CMD was constructed using stars located more than 10 arcmin from the centre of the Cetus dwarf, where the contribution of stars from Cetus is very small relative to the Galactic foreground, while the CMD of the dwarf was obtained from the inner 3 arcmin; this is presented in the left-hand panel of Fig. 2, overlaid with a series of fiducial

sequences, confirming the low metallicity of this system. The right-hand panel of this figure presents the logarithm of the density of stars associated with the dwarf as identified by the matched filter analysis, smoothed with a Gaussian kernel of 2 arcmin; note that the large blank region in the upper right-hand part of this figure is an artefact of the CCD layout of the INT/WFC. The ellipse, with semimajor and semiminor axes of 2.0 and 3.3 arcmin, encloses the peak of the stellar distribution presented in Fig. 1. The grey-scale (and contours) corresponds to the key on the right-hand side of this panel and, as presented in McConnachie & Irwin (2006), a stellar density of ∼1 star arcmin$^{-2}$ corresponds to ∼30 mag arcmin$^{-2}$. The $3\sigma$ noise limit in the stellar density map is ∼ ±2 stars arcmin$^{-2}$, resulting in a surface brightness limit of ∼29 mag arcmin$^{-2}$; hence, any extension of the dwarf leading to tidal tails should be apparent (e.g. Mayer et al. 2002). An inspection of Fig. 2 clearly reveals the presence of the Cetus dwarf itself and, as noted in McConnachie & Irwin (2006), and apparent in Fig. 1, the dwarf possesses a rather elliptical morphology; while such a non-spherical shape could potentially be interpreted as a signature of previous interactions, the lack of other evidence of interactions suggests that this is not the case and we can conclude that Cetus was formed with this morphology. Furthermore, an inspection of the stellar density in the vicinity of the main body of the dwarf uncovers no coherent, stream-like structures that could be interpreted as tidal tails and debris (cf. the magnificent tidal stream of Pal 5 as seen by Rockosi et al. 2002; Grillmair & Dionatos 2006); while there appears to be a slight signature to the lower right-hand side of the dwarf itself, it is clear from the scale of the noise over the image that this could not be considered significant.

### 3.2 Kinematics

Fig. 4 presents the distribution of Heliocentric stellar velocities obtained from the Keck/Deimos spectra, with a clear peak denoting

**Table 1.** (a) Stars observed in this survey.

| | RA | | | Dec. | | $V$ | $I$ | Velocity | $\sigma_{Vel}$ |
|---|---|---|---|---|---|---|---|---|---|
| 0 | 26 | 3.00 | −11 | 4 | 39.9 | 21.68 | 20.14 | −76.7 | 9.1 |
| 0 | 26 | 9.51 | −11 | 3 | 34.3 | 21.72 | 20.24 | −77.1 | 8.7 |
| 0 | 26 | 7.88 | −11 | 2 | 41.9 | 21.77 | 20.10 | −51.4 | 6.4 |
| 0 | 25 | 58.13 | −11 | 5 | 14.1 | 21.90 | 20.56 | −82.6 | 6.7 |
| 0 | 26 | 2.07 | −11 | 4 | 2.7 | 21.90 | 20.40 | −81.0 | 7.3 |
| 0 | 26 | 8.68 | −11 | 4 | 3.7 | 21.92 | 20.41 | −84.5 | 5.8 |
| 0 | 26 | 6.60 | −11 | 3 | 46.5 | 21.94 | 20.62 | −93.8 | 6.9 |
| 0 | 26 | 20.46 | −11 | 4 | 17.4 | 22.05 | 20.79 | −84.8 | 14.9 |
| 0 | 26 | 11.06 | −11 | 3 | 52.3 | 22.09 | 20.75 | −94.0 | 15.3 |
| 0 | 26 | 1.75 | −11 | 3 | 36.4 | 22.10 | 20.83 | −83.5 | 5.3 |
| 0 | 26 | 3.61 | −11 | 3 | 6.8 | 22.13 | 20.83 | −91.8 | 6.9 |
| 0 | 26 | 9.69 | −11 | 2 | 9.0 | 22.15 | 20.80 | −81.0 | 9.6 |
| 0 | 26 | 3.41 | −11 | 4 | 36.0 | 22.15 | 21.01 | −79.1 | 7.7 |
| 0 | 25 | 58.21 | −11 | 3 | 6.4 | 22.18 | 21.08 | −73.9 | 12.6 |
| 0 | 26 | 13.09 | −11 | 3 | 15.6 | 22.19 | 20.86 | −98.0 | 12.9 |
| 0 | 26 | 1.21 | −11 | 2 | 41.4 | 22.20 | 20.93 | −74.7 | 6.7 |
| 0 | 26 | 1.49 | −11 | 3 | 6.3 | 22.20 | 20.95 | −85.2 | 4.4 |
| 0 | 26 | 32.77 | −11 | 1 | 17.8 | 22.22 | 21.00 | −99.7 | 7.5 |
| 0 | 26 | 11.26 | −11 | 4 | 59.1 | 22.22 | 20.97 | −79.6 | 11.0 |
| 0 | 26 | 9.20 | −11 | 2 | 10.8 | 22.22 | 20.82 | −72.7 | 11.3 |
| 0 | 26 | 13.56 | −11 | 2 | 29.5 | 22.23 | 21.11 | −70.1 | 15.5 |
| 0 | 25 | 59.81 | −11 | 2 | 51.4 | 22.24 | 20.90 | −89.4 | 8.7 |
| 0 | 26 | 6.98 | −11 | 4 | 22.6 | 22.24 | 21.09 | −76.2 | 13.2 |
| 0 | 26 | 15.75 | −11 | 3 | 34.3 | 22.24 | 21.00 | −155.7 | 16.6 |
| 0 | 26 | 8.86 | −11 | 2 | 51.3 | 22.25 | 21.04 | −94.7 | 5.5 |
| 0 | 26 | 10.31 | −11 | 2 | 37.4 | 22.27 | 21.00 | −61.3 | 11.9 |
| 0 | 26 | 34.36 | −11 | 2 | 47.5 | 22.30 | 21.18 | −77.4 | 10.6 |
| 0 | 26 | 12.57 | −11 | 3 | 14.0 | 22.33 | 21.34 | −119.2 | 1.7 |
| 0 | 26 | 5.86 | −11 | 4 | 49.7 | 22.33 | 21.01 | −77.6 | 9.0 |
| 0 | 26 | 15.49 | −11 | 2 | 26.4 | 22.34 | 20.97 | −83.2 | 7.7 |
| 0 | 26 | 7.74 | −11 | 3 | 0.2 | 22.34 | 21.07 | −69.5 | 17.4 |
| 0 | 26 | 9.35 | −11 | 2 | 25.3 | 22.34 | 21.21 | −91.0 | 11.4 |
| 0 | 26 | 20.80 | −11 | 2 | 23.9 | 22.36 | 21.13 | −106.4 | 4.2 |
| 0 | 26 | 6.75 | −11 | 2 | 32.6 | 22.39 | 21.18 | −78.9 | 15.7 |
| 0 | 26 | 27.37 | −11 | 4 | 52.0 | 22.42 | 21.27 | −106.0 | 13.8 |
| 0 | 26 | 7.08 | −11 | 2 | 32.7 | 22.44 | 21.19 | −96.9 | 5.9 |
| 0 | 26 | 22.73 | −11 | 3 | 32.2 | 22.46 | 21.31 | −83.8 | 14.2 |
| 0 | 25 | 58.41 | −11 | 3 | 35.1 | 22.49 | 21.33 | −74.4 | 11.0 |
| 0 | 26 | 16.76 | −11 | 2 | 27.1 | 22.49 | 21.39 | −104.6 | 8.3 |
| 0 | 26 | 4.41 | −11 | 3 | 4.4 | 22.50 | 21.39 | −75.4 | 11.3 |
| 0 | 26 | 25.89 | −11 | 2 | 35.7 | 22.61 | 21.50 | −102.7 | 5.1 |
| 0 | 26 | 7.41 | −11 | 3 | 4.9 | 22.63 | 21.43 | −71.4 | 5.0 |
| 0 | 25 | 53.17 | −11 | 1 | 24.0 | 21.94 | 20.61 | −87.8 | 6.2 |
| 0 | 25 | 51.36 | −11 | 3 | 5.2 | 21.98 | 20.70 | −72.8 | 7.8 |
| 0 | 26 | 42.11 | −11 | 2 | 48.8 | 21.99 | 20.73 | −99.3 | 4.2 |
| 0 | 25 | 56.49 | −11 | 2 | 59.5 | 22.00 | 20.80 | −78.3 | 7.4 |
| 0 | 25 | 50.89 | −11 | 3 | 15.3 | 22.01 | 20.66 | −74.8 | 4.5 |
| 0 | 25 | 51.93 | −11 | 4 | 42.3 | 22.04 | 20.63 | −86.7 | 11.3 |
| 0 | 25 | 51.67 | −11 | 2 | 42.8 | 22.08 | 20.87 | −72.0 | 7.0 |
| 0 | 25 | 56.36 | −11 | 3 | 31.1 | 22.22 | 21.05 | −62.1 | 6.9 |
| 0 | 25 | 59.61 | −11 | 2 | 0.8 | 22.29 | 21.08 | −68.9 | 6.4 |

**Table 1.** (b) Stars observed in this survey.

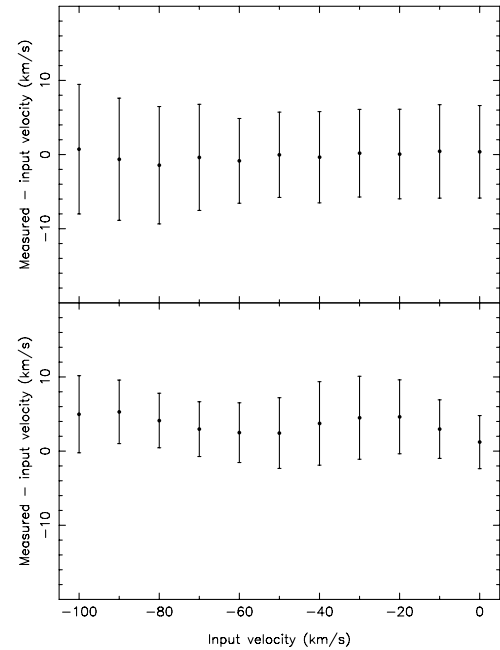| | RA | | | Dec. | | $V$ | $I$ | Velocity | $\sigma_{Vel}$ |
|---|---|---|---|---|---|---|---|---|---|
| 0 | 25 | 55.02 | −11 | 3 | 49.5 | 22.32 | 21.18 | −175.4 | 3.8 |
| 0 | 26 | 48.57 | −11 | 5 | 3.4 | 22.37 | 21.19 | 120.3 | 8.7 |
| 0 | 25 | 55.47 | −11 | 3 | 27.1 | 22.59 | 21.62 | 183.7 | 9.2 |
| 0 | 26 | 3.19 | −11 | 4 | 31.2 | 22.68 | 21.57 | −211.1 | 9.9 |
| 0 | 26 | 13.74 | −11 | 3 | 14.1 | 22.68 | 21.61 | 227.5 | 3.6 |
| 0 | 26 | 2.18 | −11 | 2 | 38.1 | 22.69 | 21.66 | −56.1 | 7.2 |
| 0 | 25 | 57.69 | −11 | 3 | 5.7 | 22.71 | 21.58 | −88.7 | 9.6 |
| 0 | 26 | 18.48 | −11 | 3 | 19.0 | 22.76 | 21.62 | −123.3 | 5.7 |
| 0 | 25 | 56.72 | −11 | 2 | 36.0 | 22.78 | 21.55 | 172.5 | 7.4 |
| 0 | 25 | 53.76 | −11 | 1 | 46.8 | 22.79 | 21.70 | −91.5 | 15.3 |
| 0 | 26 | 50.97 | −11 | 3 | 47.3 | 22.80 | 21.62 | 117.4 | 8.6 |
| 0 | 26 | 26.24 | −11 | 2 | 7.3 | 22.89 | 21.70 | −104.9 | 8.8 |
| 0 | 25 | 54.15 | −11 | 5 | 35.4 | 22.89 | 21.97 | 189.6 | 4.6 |
| 0 | 26 | 8.15 | −11 | 3 | 7.7 | 22.91 | 21.85 | −71.4 | 6.3 |
| 0 | 25 | 46.41 | −11 | 3 | 51.8 | 22.94 | 21.84 | 253.5 | 12.9 |
| 0 | 25 | 59.34 | −11 | 2 | 5.6 | 22.96 | 21.99 | −119.4 | 17.9 |
| 0 | 25 | 54.71 | −11 | 3 | 0.5 | 22.99 | 21.94 | −129.5 | 2.7 |
| 0 | 26 | 40.69 | −11 | 2 | 24.6 | 23.00 | 21.83 | −51.6 | 7.2 |
| 0 | 25 | 57.79 | −11 | 1 | 13.9 | 23.09 | 21.61 | 2.6 | 6.4 |



**Figure 3.** The systematic error in velocity as determined from the analysis of synthetic spectra, using sky residuals as determined from the data. The error bars represent the uncertainty in the velocity determination. The top panel uses Poisson sampling of the median sky, whereas the the lower panel uses the median skies from separate CCDs. The overall results show no substantial velocity systematics in the range of $-100 \rightarrow 0\,\mathrm{km\,s^{-1}}$, and are typically $\sim 1\,\mathrm{km\,s^{-1}}$ in the upper panel, increasing to $\sim 4$–$5\,\mathrm{km\,s^{-1}}$ in the lower panel.

the presence of the Cetus dwarf galaxy. Overplotted in this figure is the best-fitting Gaussian, with a systemic velocity of $-85\,\mathrm{km\,s^{-1}}$ and width of $15\,\mathrm{km\,s^{-1}}$; note that this is inconsistent with velocities of three H I clumps ($-311$, $-268$ and $-262\,\mathrm{km\,s^{-1}}$) in the vicinity of Cetus as measured by Bouchard, Carignan & Staveley-Smith (2006), and it must be concluded that they do not represent Cetus' gas content. Following Richstone & Tremaine (1986), we assume that the Cetus dwarf can be represented as a simple, spherically symmetric stellar system of central surface brightness $\Sigma_\mathrm{o}$,

half-brightness radius of $r_\mathrm{hb}$ and velocity dispersion $\sigma$ and can then estimate the mass-to-light ratio ($M/L$) in the system to be

$$\frac{M}{L} = \eta \, \frac{9}{2\pi G} \, \frac{\sigma^2}{\Sigma_\mathrm{o} r_\mathrm{hb}}, \qquad (1)$$

where $\eta$ is a dimensionless structure parameter which has a typical value of $\sim$unity; this formula assumes that mass traces light within the dwarf.
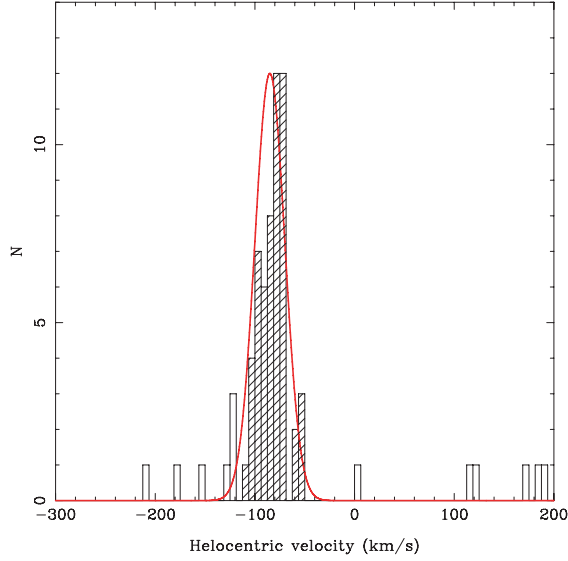
**Figure 4.** The distribution of stellar velocities obtained in this survey; a clear overdensity, denoting the systemic velocity of the Cetus dwarf, is clearly visible, with a negligible contamination from the Galaxy. The overplotted solid line is a Gaussian fit to the data, assuming a systemic velocity of $-85\,\mathrm{km\,s^{-1}}$ and a width of $15\,\mathrm{km\,s^{-1}}$. The dashed histogram highlights those stars within $\pm30\,\mathrm{km\,s^{-1}}$ of the systemic velocity.



**Figure 5.** The left-hand panel presents the likelihood contours (at $1, 2$ and $3\sigma$) for the mean and dispersion of the radial velocities of the Cetus dwarf populations. The black curves represent the entire sample, while the lighter curves (red online) represent stars within 5 arcmin of the centre of the dwarf. The right-hand panel presents the relative likelihood curves for the $M/L$ of the dwarf (given the same selection as the left-hand panel); both peak strongly in the region of $M/L \sim 70$.

Fig. 5 presents the results of a likelihood calculation for this population of RGB stars. First, the right-hand panel presents contours at $1, 2$ and $3\sigma$ of the mean velocity and velocity dispersion of this population, consistent with the fit values presented in Fig. 4. The dark line in this figure corresponds to the entire RGB sample, whereas the lighter line utilizes only those stars within 5 arcmin of the centre of the dwarf; the results of this analysis suggest that the systemic velocity of Cetus is $-87 \pm 2\,\mathrm{km\,s^{-1}}$ with an internal velocity dispersion of $17 \pm 2\,\mathrm{km\,s^{-1}}$. The left-hand panel presents the relative likelihood for the $M/L$ of the Cetus dwarf, clearly peaking at an $M/L \sim 70$.

### 3.3 Spectroscopic metallicities

The equivalent widths (EWs) of the CaT can be used as a proxy measure of the stellar metallicity. As with our previous Keck/Deimos studies (e.g. Ibata et al. 2005), the approach of Rutledge, Hesser &

Stetson (1997) is adopted, with

$$\left[\frac{\mathrm{Fe}}{\mathrm{H}}\right] = -2.66 + 0.42\left[\sum\mathrm{Ca} - 0.64(V_{\mathrm{HB}} - V)\right] \quad (2)$$

where

$$\sum\mathrm{Ca} = 0.5\mathrm{EW}_{\lambda 8498} + \mathrm{EW}_{\lambda 8542} + 0.6\mathrm{EW}_{\lambda 8662} \quad (3)$$

and $(V_{\mathrm{HB}} - V)$ provides a surface gravity correction term; for Cetus $V_{\mathrm{HB}} = 25.10$, scaled from the M31 value employed by Ibata et al. (2005). The spectroscopically derived metallicities are presented as colour-coded points superimposed on the left-hand panel of Fig. 2; the solid circles in this figure denote stars within $30\,\mathrm{km\,s^{-1}}$ of the systemic velocity, whereas the open circles are the remaining stars in the sample. The errors on the metallicity measures are $\sim0.2$. The stars overlay several fiducial tracks of systems with determined metallicities (which are colour-coded on the same scheme as the stars). A comparison of the stellar metallicities and the fiducial tracks reveal that the two measures are consistent and that the Cetus dwarf galaxy is dominated by an old, metal-poor population with $[\mathrm{Fe}/\mathrm{H}] \sim -1.9$, as per the findings of Whiting et al. (1999).

### 3.4 A hint of rotation

Fig. 6 presents the spatial distribution of stars along the major axis, with velocities within $30\,\mathrm{km\,s^{-1}}$ of the systemic (filled circles). An eye-ball examination of this figure reveals that there appears to be a velocity offset between those stars to the right- and left-hand side of the dwarf centre, with those at positive distances possessing a more negative velocity than those at negative distance. Noting the errors to the data points, the signature is somewhat tentative and hence no rigorous kinematic model fitting was undertaken. As an illustration, a simple constant rotational velocity profile was fitted to the stars within 5 arcmin of the centre of the dwarf, with a resultant best-fitting rotational velocity of $7.7 \pm 1.2\,\mathrm{km\,s^{-1}}$; this rotation curve is overplotted as a solid line in Fig. 6 as well as two additional fiducial rotation curves of 0 and $15\,\mathrm{km\,s^{-1}}$. The dotted line represents a linear model, representing solid body rotation, with a best fit of $2.5 \pm 0.4\,\mathrm{km\,s^{-1}}\,\mathrm{arcmin^{-1}}$. In removing the signature of the best-fitting constant rotation velocity, the velocity dispersion within the inner 5 arcmin falls to $14\,\mathrm{km\,s^{-1}}$ with a $4\sigma$ clipping), and to $8\,\mathrm{km\,s^{-1}}$



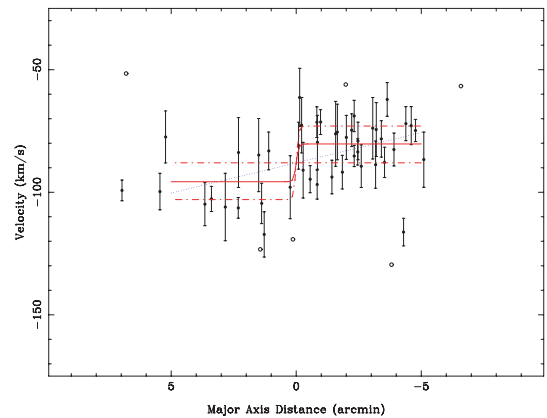**Figure 6.** The spatial distribution of stars along the major axis of the Cetus dwarf galaxy. The solid points denote stars within $30\,\mathrm{km\,s^{-1}}$ of the systemic velocity. The solid line represents the best-fitting rotational velocity of $7.7\,\mathrm{km\,s^{-1}}$, with the dot–dashed line representing fiducial rotation velocities of 0 and $15\,\mathrm{km\,s^{-1}}$. The dotted line presents a linear model, representing solid body rotation, with a best fit of $2.5 \pm 0.4\,\mathrm{km\,s^{-1}}\,\mathrm{arcmin^{-1}}$.

when applying a more stringent $2\sigma$ clipping. Hence, if real, the rotation of Cetus represents a significant kinematic component in this system.

### 3.5 Constraints on the Local Group

As noted previously, Cetus is one of only two isolated dSph galaxies in the Local Group. Hence, measurement of its heliocentric velocity provides a vital constraint on its orbit through the Local Group, under reasonable assumptions about its proper motion and the mass distribution of the Local Group.

In estimating the Local Group velocity, $v_{lg}$, of Cetus, the first step involves transforming its heliocentric velocity into a galactocentric radial velocity, finding $v_g = -25 \, \mathrm{km \, s^{-1}}$. It is assumed that the Milky Way and M31 account for all the mass of the Local Group, and that their mass ratio is $a = 1$. Einasto & Lynden-Bell (1982) presented arguments which suggest that the total angular momentum of the Local Group is close to zero, which requires that these two galaxies are on a nearly radial orbit with respect to one another. If Cetus is on a purely radial orbit with respect to the centre of mass of the Local Group, then its radial velocity, $v_{lg}$, is constrained by

$$\boldsymbol{v}_{lg} \cdot \hat{\boldsymbol{r}} = v_g - \boldsymbol{v}_{mw} \cdot \hat{\boldsymbol{r}}. \tag{4}$$

where $\hat{\boldsymbol{r}}$ is the unit vector in the direction of Cetus and $\boldsymbol{v}_{mw}$ is the Local Group velocity of the Milky Way ($\boldsymbol{v}_{mw} = -61.5 \, \mathrm{km \, s^{-1}}$ for $a = 1$). If it is assumed that Cetus is moving radially away from the centre of the Local Group, then $v_{lg} = 14 \, \mathrm{km \, s^{-1}}$, at a barycentric distance of 602 kpc.

Fig. 7 shows the Local Group velocity of Cetus plotted against its barycentric distance. Also shown as the open circles (red online) are other candidate isolated Local Group dwarf galaxies, while the open squares (blue online) represent galaxies belonging to other nearby groups. The dark-grey and light-grey solid circles (magenta and green online, respectively) represent dwarf galaxies which are satellites of M31 and the Milky Way, respectively. For these galaxies,
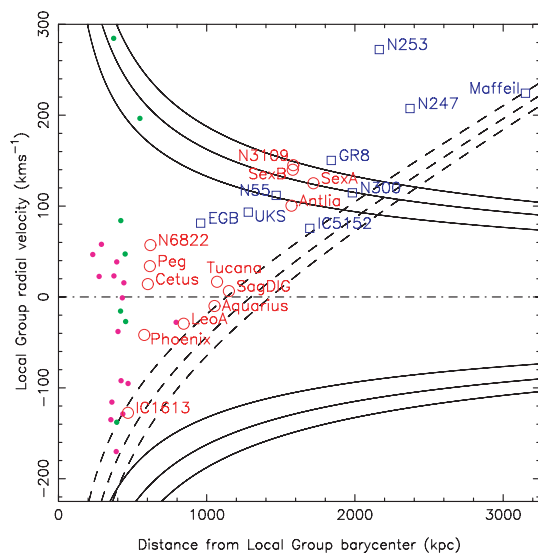


**Figure 7.** The barycentric Local Group distance versus the Local Group radial velocity for various dwarfs in the local universe. Here, the open circles (red online) are other candidate isolated Local Group dwarf galaxies, the open squares (blue online) represent galaxies belonging to other nearby groups, while the dark-grey and light-grey solid circles (magenta and green online, respectively) represent dwarf galaxies which are satellites of M31 and the Milky Way, respectively.

the approximation that their dynamics are governed by the net Local Group potential is not valid, and so the velocities derived will not be with respect to the Local Group centre of mass. The dot–dashed line represents the apocentre of orbits in the Local Group and the dashed curves represent the maximum distance that a galaxy could reach, given its current velocity for a total Local Group mass of 2, 3 and $4 \times 10^{12} \, \mathrm{M_\odot}$ (inner to outer curves). The solid curves represent the escape velocity of the Local Group for these masses. Thus, galaxies which are above the top set of solid lines or below the bottom set of solid lines cannot be bound to the Local Group. Likewise, galaxies to the right-hand side of the dashed curves would not have been able to reach their position if they are Local Group members (Irwin 1999).

Several interesting results are immediately apparent in Fig. 7; Cetus is close to the apocentre of its orbit in the Local Group, while the other isolated dSph, Tucana, is similarly at apocentre, along with the Sagittarius dIrr and the transition galaxy Aquarius (DDO210). The Sagittarius dIrr and Aquarius could only have reached their current positions if the mass of the Local Group is $\gtrsim 2 \times 10^{12} \, \mathrm{M_\odot}$, and they are on very radial orbits. There is some overlap in this plot between Local Group galaxies and members of nearby groups, which reflects the well-known result that there are no distinct boundaries between the hundred or so groups which form the Local Supercluster. Particularly, the Sculptor group joins with the Local Group via a bridge of galaxies including NGC 55, UKS 2323-326 and IC 5152. Sextans A, B, Antlia and NGC 3109 form a distinct grouping in the sky (the NGC 3109 group). Fig. 7 shows that they are dynamically distinct from other Local Group galaxies and that they can only be bound to the Local Group if its mass is $\gtrsim 4 \times 10^{12} \, \mathrm{M_\odot}$.

## 4 CONCLUSIONS

This paper has presented a study of the Cetus dwarf galaxy, utilizing a matched filter analysis of the INT/WFC observations of Cetus dwarf galaxy presented by McConnachie et al. (2005). The results of this analysis, however, suggest that Cetus does not possess the extratidal stars indicative of any significant interaction in the past. Hence, it can be concluded that Cetus truly does represent a lonely and isolated member of the Local Group.

In addition, this paper has presented a spectroscopic survey of the Cetus dwarf, utilizing a kinematic survey to study its dynamical properties. A maximum-likelihood analysis of the kinematic sample reveals that Cetus has a systemic velocity of $-87 \pm 2 \, \mathrm{km \, s^{-1}}$ and an internal velocity dispersion of $17 \pm 2 \, \mathrm{km \, s^{-1}}$. Furthermore, a viral analysis of these data suggests that this dwarf possesses an $M/L \sim 70$ (assuming mass traces light); however, this result may be misleading as the data tentatively reveal the presence of some rotation with a best-fitting rotational velocity of $7.7 \pm 1.2 \, \mathrm{km \, s^{-1}}$; removing this rotation results in a velocity dispersion between 8 and $14 \, \mathrm{km \, s^{-1}}$, depending on the statistical clipping. As ever, more data and accurate kinematic modelling will be required to fully address these issues. Finally, an analysis of Cetus' orbit through the Local Group finds it to be at apocentre, providing a weak additional constraint to the mass of the Local Group. Taken in conjunction with the other members of the dwarf population in the local universe, the mass of the Local Group is found to be $\gtrsim 2 \times 10^{12} \, \mathrm{M_\odot}$.

## ACKNOWLEDGMENTS

## REFERENCES

Belokurov V. et al., 2006a, ApJ, 642, L137
Belokurov V. et al., 2006b, ApJ, 647, L111
Bouchard A., Carignan C., Staveley-Smith L., 2006, AJ, 131, 2913
Einasto J., Lynden-Bell D., 1982, MNRAS, 199, 67
Einasto J., Kaasik A., Saar E., 1974, Nat, 250, 309
Faber S. M. et al., 2003, SPIE, 4841, 1657
Freeman K., Bland-Hawthorn J., 2002, ARA&A, 40, 487
Grillmair C. J., Dionatos O., 2006, ApJ, 641, L37
Ibata R. A., Gilmore G., Irwin M. J., 1994, Nat, 370, 194
Ibata R., Irwin M., Lewis G., Ferguson A. M. N., Tanvir N., 2001, Nat, 412, 49
Ibata R., Chapman S., Ferguson A. M. N., Lewis G., Irwin M., Tanvir N., 2005, ApJ, 634, 287
Irwin M., 1999, IAUS, 192, 409
Johnston K. V., Choi P. I., Guhathakurta P., 2002, AJ, 124, 127
Kepner J., Fan X., Bahcall N., Gunn J., Lupton R., Xu G., 1999, ApJ, 517, 78
Klypin A., Kravtsov A. V., Valenzuela O., Prada F., 1999, ApJ, 522, 82
Martin N. F., Ibata R. A., Bellazzini M., Irwin M. J., Lewis G. F., Dehnen W., 2004, MNRAS, 348, 12
Mateo M. L., 1998, ARA&A, 36, 435
Mayer L., Governato F., Colpi M., Moore B., Quinn T., Wadsley J., Stadel J., Lake G., 2001a, ApJ, 559, 754
Mayer L., Governato F., Colpi M., Moore B., Quinn T., Wadsley J., Stadel J., Lake G., 2001b, ApJ, 547, L123
Mayer L., Moore B., Quinn T., Governato F., Stadel J., 2002, MNRAS, 336, 119
Mayer L., Mastropietro C., Wadsley J., Stadel J., Moore B., 2006, MNRAS, 369, 1021
McConnachie A. W., Irwin M. J., 2006, MNRAS, 365, 1263
McConnachie A. W., Irwin M. J., Ferguson A. M. N., Ibata R. A., Lewis G. F., Tanvir N., 2005, MNRAS, 356, 979
McConnachie A. W., Arimoto N., Irwin M. J., Tolstoy E., 2006, MNRAS, 373, 715
Moore B., Ghigna S., Governato F., Lake G., Quinn T., Stadel J., Tozzi P., 1999, ApJ, 524, L19
Richstone D. O., Tremaine S., 1986, AJ, 92, 72
Robin A. C., Reylé C., Derrière S., Picaud S., 2003, A&A, 409, 523
Rockosi C. M. et al., 2002, AJ, 124, 349
Rutledge G. A., Hesser J. E., Stetson P. B., 1997, PASP, 109, 907
Sarajedini A. et al., 2002, ApJ, 567, 915
Stoehr F., White S. D. M., Tormen G., Springel V., 2002, MNRAS, 335, L84
Venn K. A., Irwin M., Shetrone M. D., Tout C. A., Hill V., Tolstoy E., 2004, AJ, 128, 1177
White S. D. M., Rees M. J., 1978, MNRAS, 183, 341
Whiting A. B., Hau G. K. T., Irwin M., 1999, AJ, 118, 2767
Willman B. et al., 2005a, ApJ, 626, L85
Willman B. et al., 2005b, AJ, 129, 2692
Zucker D. B. et al., 2004, ApJ, 612, L121
Zucker D. B. et al., 2006a, ApJ, 643, L103
Zucker D. B. et al., 2006b, ApJ, 650, L41

This paper has been typeset from a TeX/LaTeX file prepared by the author.